

Naval Research Laboratory

Washington, DC 20375-5320



NRL/MR/6750--94-7461

AD-A278 758



Analysis of Recent Agile Mirror Data

J. MATHEW
R. A. MEGER

*Charged Particle Physics Branch
Plasma Physics Division*

J. A. GREGOR

*University of Maryland
College Park, MD*



March 28, 1994

47P8 94-13224



Approved for public release; distribution unlimited.

94 5 02 100

REPORT DOCUMENTATION PAGE

*Form Approved
OMB No. 0704-0188*

Public reporting burden for this collection of information is estimated to average 1 hour per response, including the time for reviewing instructions, searching existing data sources, gathering and maintaining the data needed, and completing and reviewing the collection of information. Send comments regarding this burden estimate or any other aspect of this collection of information, including suggestions for reducing this burden, to Washington Headquarters Services, Directorate for Information Operations and Reports, 1215 Jefferson Davis Highway, Suite 1204, Arlington, VA 22202-4302, and to the Office of Management and Budget, Paperwork Reduction Project (0704-0188), Washington, DC 20503.

1. AGENCY USE ONLY (Leave Blank)	2. REPORT DATE	3. REPORT TYPE AND DATES COVERED	
	March 28, 1994	Interim	
4. TITLE AND SUBTITLE Analysis of Recent Agile Mirror Data			5. FUNDING NUMBERS PE - 61153N
6. AUTHOR(S) J. Mathew, J.A. Gregor,* and R.A. Meger			
7. PERFORMING ORGANIZATION NAME(S) AND ADDRESS(ES) Naval Research Laboratory Washington, DC 20375-5320			8. PERFORMING ORGANIZATION REPORT NUMBER NRL/MR/6750-94-7461
9. SPONSORING/MONITORING AGENCY NAME(S) AND ADDRESS(ES) Office of Naval Research 800 N Quincy Street Arlington, VA 22217-5660			10. SPONSORING/MONITORING AGENCY REPORT NUMBER
11. SUPPLEMENTARY NOTES *University of Maryland, College Park, MD			
12a. DISTRIBUTION/AVAILABILITY STATEMENT Approved for public release; distribution unlimited.		12b. DISTRIBUTION CODE	
13. ABSTRACT (Maximum 200 words) Recent data taken with the agile mirror hollow cathode setup using a crossatron driven pulser show that acceptable reflected X-band microwave signals can be obtained under a narrow range of experimental parameters. The 15-cm x 25-cm x 1-cm planar discharge in 150 mTorr of air yields quite reproducible results in the presence of an axial magnetic field of ~ 100 Gauss. The discharge tends to turn off around 150 μ s, but if the voltage is left on, the discharge restrikes after ~ 0.5 ms. The turn-off is not observed at higher pressure, but the reflected microwave signals show time variations at these pressures. It is believed that the dimensions of the present hollow cathode are not optimal. A cathode with an adjustable cavity is being built to investigate the scaling of the cathode dimensions with pressure and magnetic field for the full size 50-cm x 50-cm agile mirror experiment. There are some indications that, particularly at the lower pressures, the discharge column is beam dominated.			
14. SUBJECT TERMS Agile mirror Data Analysis			15. NUMBER OF PAGES 48
			16. PRICE CODE
17. SECURITY CLASSIFICATION OF REPORT UNCLASSIFIED	18. SECURITY CLASSIFICATION OF THIS PAGE UNCLASSIFIED	19. SECURITY CLASSIFICATION OF ABSTRACT UNCLASSIFIED	20. LIMITATION OF ABSTRACT UL

CONTENTS

I.	INTRODUCTION	1
II.	DATA SUMMARY	1
III.	DATA ANALYSIS	4
A.	POSITIVE COLUMN	4
1.	Electron Temperature	5
2.	Electric Field	7
3.	Diffusion Coefficient	8
4.	Ion Gyroradius	13
5.	Filamentation	13
6.	Interpretation of Data	14
B.	CATHODE LAYER	16
1.	Hollow Cathode	16
2.	Sputtering	18
3.	Cathode Fall	19
4.	Free Fall Theory	22
5.	Mobility Theory	23
6.	Self Sustainment Condition	24
7.	Interpretation of Data	26
IV.	SUMMARY OF RESULTS	28
	REFERENCES	30

A-1		Codes and/or Special
Dist		

ANALYSIS OF RECENT AGILE MIRROR DATA

I. INTRODUCTION

Recent interest in developing electronically steered plasma reflectors for microwave beams,¹ resulted in a proof of principle experiment² that demonstrated that a planar plasma mirror can be formed with characteristics approaching those desired for an X-band reflector. This report presents a selection of recent data obtained with the agile mirror setup described in Ref. 2. Following the data summary in Section II, a somewhat detailed analysis of the data appears in Section III. The analysis arrives at preliminary estimates of the various plasma parameters, and attempts to develop a rationale for future experiments. Finally, Section IV contains some conclusions and a brief description of planned experiments.

II. DATA SUMMARY

Recent data taken with the agile mirror hollow cathode setup used a newly built power supply which incorporated a crossatron switch to provide square voltage pulses with variable pulse duration and duty cycle. The power supply can operate in a burst mode or in a free-running mode. The pulse repetition rate in the free-running mode can be varied from 0.1 Hz to 10 Hz. For the data in this report, the free-running mode was chosen and the pulse repetition rate was 1 Hz. Figure 1(a) shows a simplified circuit diagram of the power supply used to drive the plasma mirror. The energy storage capacitor C has a capacitance value of $20 \mu\text{F}$, and the series resistance R controls the V-I characteristic of the circuit. Figure 1(b) shows a sketch of the hollow cathode cross section. The hollow cathode is a

U-shaped brass electrode supported by a Lucite holder. The rectangular cathode cavity is 1.2 cm deep, 1.6 cm wide and 15.5 cm long. A 1.8 cm \times 15.0 cm collimating slot in a Lucite plate placed 3 mm from the cathode enables the development of a well defined planar discharge. A 100-mW X-band sweeper is used to determine the mirror reflectivity.

Figure 2 shows the data obtained with a series resistance of 180 Ω . Ch. 1 is the voltage across the plasma discharge. It is uncalibrated for this figure, but its sensitivity is 10 kV/volt for all subsequent figures. Ch. 2 is the discharge current. Its sensitivity is 100 A/volt. Ch. 3 is the reflected microwave signal measured with an uncalibrated crystal detector. Ch. 4 is the transmitted signal (thru-transmission) measured with a negative polarity crystal detector. Figure 2 shows that the signal on Ch. 4 goes from the -5 mV level to zero when the plasma mirror is turned on. This represents cutoff of the transmitted microwaves. The power supply charging voltage is 3 kV in Fig. 2. The magnetic field is 98 Gauss and the pressure is 150 mTorr (air). Coil currents of 15, 20 and 25 A correspond to field strengths of 98, 130 and 163 Gauss. The time scale is 20 μ s/div. The reflected microwave signal is seen to be flat for at least 70 μ s. Conditions such as in Fig. 2 are realized under a narrow range of experimental parameters. Similar data is shown in Fig. 3 for a 100- Ω series resistance. The voltage pulse is 400 μ s long, but the discharge appears to be switching to a low current state at about 120 μ s. A series resistance stabilizes the discharge. When the current drops, the voltage across the discharge rises due to the presence of the resistance. This prevents the current from dropping any further. The value of the series resistance does not markedly affect the intrinsic V-I characteristics of the discharge. This is illustrated by Figs. 4(a) and 5(a). Figure 4(a) shows the V-I

characteristics for three values of the series resistance, and Fig. 4(b) is for four different pressures. Figure 5 shows the current dependence of the plasma resistance for various pressures and series resistances. The plasma resistance is computed by dividing the voltage across the discharge by the current. These characteristics were compiled from a sequence of shots by recording the voltage and current at $80 \mu\text{s}$ where the signals appeared to be quite flat. For most of the data analysis that follows, a point on the V-I characteristics at 8 A and 1.4 kV (plasma voltage) is chosen.

The discharge current turn-off feature seen in Fig. 3 is observed only when the magnetic field is present. Figure 6 shows the exception to this rule. The discharge oscillates between the patterns in Figs. 6(a) and 6(b) at the 1 Hz rep rate. If the charge voltage is raised, the discharge current takes the form in Fig. 7(a). Figures 7 thru 9 show the effect of the magnetic field. The series resistance in Fig. 7 is 40Ω . It is 100Ω in Fig. 8 and 200Ω in Fig. 9.

Electron density measurements were attempted at the low discharge currents by measuring the microwave cutoff frequency. Since the crystal detector was extremely sensitive to frequency changes, the microwave frequency was kept fixed for a particular run. Instead, the pressure was dropped until the reflected microwave signal disappeared. Figure 10 shows three shots taken at slightly different pressures. The series resistance is 200Ω . The currents and pressures where the reflected signal is very small are recorded and the results are shown in Fig. 11 for three different microwave frequencies corresponding to electron densities of 1×10^{12} , 1.14×10^{12} and $1.55 \times 10^{12} \text{ cm}^{-3}$. At around 133 mTorr, the discharge switches from a low current to a high current discharge. Figure 12 captures

the situation corresponding to the exact pressure where the transition occurs. It appears from the reflected signal that the density is also increasing as the current is increasing.

III. DATA ANALYSIS

The data presented in the previous section is analyzed here to develop a self consistent model and arrive at preliminary estimates of the various plasma parameters describing the mirror discharge. The analysis is divided into two sections. Section A deals with the positive column from which microwaves are reflected. Section B treats the cathode layer of the hollow cathode. The physical processes occurring in this layer profoundly influence the discharge characteristics and the nature of the positive column. It is easier to start with the analysis of the positive column because once the voltage across the column is determined, it can be subtracted from the discharge voltage to give the cathode fall voltage. This voltage needs to be known before any analysis of the cathode layer can be initiated. The last subsections within Section A and B deal specifically with interpreting various features in the experimental data within the framework of the self consistent model developed in the previous subsections.

A. POSITIVE COLUMN

The positive column merely serves to provide electrical continuity between the cathode layer and the anode. Quasineutrality prevails in the column, i.e. $n_e \approx n_i \approx n$. (Negative ions are neglected for the sake of simplicity.) The charged particle density n in the column is described by the relation

$$D_a \nabla^2 n + \nu_i n - \beta n^2 = \frac{\partial n}{\partial t}, \quad (1)$$

where D_a is the ambipolar diffusion coefficient in the presence of the axial magnetic field, ν_i is the ionization frequency and β is the dissociative recombination coefficient. CGS Gaussian units are used in this report. The Townsend ionization coefficient α is related to ν_i by $\alpha = \nu_i/v_{de}$, where v_{de} is the electron drift velocity.

Density gradients along the magnetic field are negligibly small because of the large electron drift velocity due to the axial electric field E . The strongest density gradient is across the thickness of the plasma mirror. If x is the coordinate describing the mirror thickness, then Eq. (1) becomes under steady state conditions

$$D_a \frac{\partial^2 n}{\partial x^2} + \nu_i n - \beta n^2 = 0. \quad (2)$$

This differential equation does not have a closed form solution because of the presence of the n^2 term. Equation (2) is appropriate for a thermal plasma. If ionization processes in the positive column are substantially influenced by high energy electrons (beams), Eq. (2) ceases to be valid. This possibility is addressed in Section A3.

1. Electron Temperature

If the density profile $n(x)$ is reasonably flat at the center, $x = 0$, then $\partial^2 n / \partial x^2$ can be ignored. The central density is then given by $n = \nu_i / \beta$. The ionization frequency ν_i and the recombination coefficient β are functions of the electron temperature T_e . If T_e is known, the central density can be evaluated. Alternatively, if the density is known, the

temperature can be determined. Extrapolating the data of Fig. 11, the electron density at 8 Å and 150 mTorr is roughly $2 \times 10^{12} \text{ cm}^{-3}$. Electron impact ionization is achieved by electrons in the high energy tail of the electron distribution function. $\nu_i(T_e)$ is described by the relation³

$$\nu_i = N\bar{v}C_i [I + 2kT_e] \exp\left(\frac{-I}{kT_e}\right), \quad (3)$$

where the electron distribution function is assumed to be a Maxwellian shifted in velocity space by the drift velocity. The drift velocity is usually much smaller than the random velocity. N is the gas density and \bar{v} is the mean electron velocity, i.e. $\bar{v} = \sqrt{8kT_e/(m\pi)}$. C_i is a constant defined in Ref. 3. Its value for Nitrogen is $0.85 \times 10^{-17} \text{ cm}^2/\text{eV}$ and the ionization potential I is 15.6 eV. At 150 mTorr, $N = 5.3 \times 10^{15} \text{ cm}^{-3}$. Solving $\nu_i(T_e) - n\beta(T_e) = 0$ by trial and error, $T_e = 2.1 \text{ eV}$. This means that a self consistent solution is for the plasma to have an electron temperature of 2.1 eV which implies that $\beta = 2 \times 10^{-8} \text{ cm}^3/\text{s}$ for N_2 , and $\nu_i = 6 \times 10^4 \text{ Hz}$. Therefore $\nu_i/p = 4 \times 10^5 \text{ Torr}^{-1}\text{s}^{-1}$.

If high energy electrons from the cathode play an important role in the impact ionization processes within the positive column, then the electron distribution function is no longer a Maxwellian. Superimposed over the thermal component (Maxwellian), the distribution function could have a high energy tail or a distinct high energy beam component. In either case, because of the increased ionization by high energy electrons, the equilibrium condition $n\beta = \nu_i$ may be satisfied at a much lower electron temperature for the thermal component of the electron distribution.

Another important effect is the role played by metastables.⁴ One of the metastable

states of N₂ has an excitation energy of 8.4 eV which is considerably less than the ionization potential, 15.6 eV. Hence a larger proportion of electrons can create metastables. It is also easier to ionize a metastable molecule because it is already in the excited state. This two step ionization process is important because although there are many fewer metastables than ground state atoms, this is offset by the larger number of electrons which could ionize the metastables. Another notable process in nitrogen is metastable-metastable ionization⁴ where the combined energy of two metastables exceeds the ionization potential, resulting in an ionized N₂ molecule. Again, the net result of these processes is a lower calculated electron temperature for the positive column.

2. Electric Field

The electric field within the positive column may be computed in three ways. The first approach uses the value of the current density in the positive column, where it is known that most of the current is carried by electrons. Assuming that the positive column is 1 cm thick and 15 cm wide, a discharge current of 8 A implies $j = 0.53 \text{ A/cm}^2$. Since $j = nev_{de}$, the electron drift velocity $v_{de} = 1.6 \times 10^6 \text{ cm/s}$ if n is assumed to be $2 \times 10^{12} \text{ cm}^{-3}$ using the data in Fig. 11. Referring to experimental data³ on v_{de} , $E/p = 2.5 \text{ V cm}^{-1}\text{Torr}^{-1}$. If a portion of the current is carried by a beam of high energy electrons, the current density of the thermal plasma component will be smaller, which means that v_{de} and E/p will be correspondingly smaller.

Another way of estimating E/p is to use the value for the ionization frequency ν_i that is required for maintaining the desired electron density in the positive column (see Section A1). Since $\nu_i/p = (\alpha/p)v_{de}$ (α being the Townsend ionization coefficient), ν_i/p

is a function of E/p because both α/p and v_{de} are functions of E/p , and experimental data on α/p and v_{de} are readily available (see for example Ref. 3). This dependence of ν_i/p on E/p is particularly strong, and if ν_i/p is known, E/p can be determined. When $E/p = 44 \text{ V cm}^{-1}\text{Torr}^{-1}$, $v_{de} = 1.13 \times 10^7 \text{ cm/s}$, $\alpha/p = 0.032 \text{ cm}^{-1}\text{Torr}^{-1}$ for air, and $\nu_i/p = 3.6 \times 10^5 \text{ s}^{-1}\text{Torr}^{-1}$ which is close to the value 4×10^5 obtained in Section A1. E/p is therefore $44 \text{ V cm}^{-1}\text{Torr}^{-1}$, but this value for E/p is too high when compared with the value of $2.5 \text{ V cm}^{-1}\text{Torr}^{-1}$ obtained above. This discrepancy may be resolved if it is assumed that the electron distribution function has a distinct high energy component on top of the usual Maxwellian distribution. Because of the added ionization provided by the high energy electrons, ν_i/p of the thermal plasma component could be much lower and hence E/p could be correspondingly smaller.

A third way of computing E/p is to use the electron temperature and the relation⁵ $T_e = 8 [10^{14}(E/N)]^{1/2}$ where T_e is in eV. Using 2.1 eV for T_e (see Section A1), $E/p = 23 \text{ V cm}^{-1}\text{Torr}^{-1}$ which also appears to be high. T_e needs to be 0.7 eV to yield $E/p = 2.5 \text{ V cm}^{-1}\text{Torr}^{-1}$ which was the value obtained using the current density. A low T_e implies that the role of high energy electrons may be quite significant in the positive column (see Section A1). The lack of agreement between the three values of E/p suggests that high energy electron beams are responsible for a substantial amount of ionization within the positive column. This possibility is discussed in more detail under Section B3.

3. Diffusion Coefficient

The importance of the diffusion term in Eq. 2 needs to be determined. D_a represents the ambipolar diffusion coefficient perpendicular to the axial magnetic field. D_a is related

to the individual diffusion coefficients $D_{\perp e}$ and $D_{\perp i}$ of electrons and ions.

$$D_a = \frac{\mu_{\perp i} D_{\perp e} + \mu_{\perp e} D_{\perp i}}{\mu_{\perp i} + \mu_{\perp e}} \quad (4)$$

In the presence of a magnetic field B , the mobility perpendicular to B is given by⁶

$$\mu_{\perp e} = \frac{\mu_{oe} \nu_{me}^2}{\nu_{me}^2 + \omega_{ce}^2}, \quad (5)$$

where μ_{oe} is the mobility in the absence of a magnetic field i.e. $\mu_{oe} = e/(m_e \nu_{me})$, ν_{me} is the effective collision frequency of electrons for momentum transfer (it is predominantly the electron-neutral collision frequency ν_{en}), and the electron cyclotron frequency $\omega_{ce} = eB/(m_e c)$. An equation similar to (5) can be written for ions. The diffusion coefficient

$$D_{\perp i} = \frac{D_{oi} \nu_{mi}^2}{\nu_{mi}^2 + \omega_{ci}^2}, \quad (6)$$

where D_{oi} is the diffusion coefficient in the absence of the magnetic field. Since $D = (kT/e)\mu$, $D_{oi} = kT_i/(m_i \nu_{mi})$. An equation similar to (6) can also be written for electrons.

However, in many plasma experiments the classical diffusion coefficient for electrons is several orders of magnitude less than the observed diffusion coefficient. (There are some experiments, however, where classical diffusion perpendicular to the magnetic field has been observed.) Bohm postulated a diffusion coefficient⁷ scaling as $1/B$ (instead of the classical $1/B^2$ scaling) to obtain agreement with the spreading observed in a discharge in argon between a thermionically heated cathode filament and a graphite anode. A collimating slot 12.7 mm \times 3.2 mm just after the filament defined the transverse dimensions of the 12-cm long discharge in Bohm's experiment. The pressure was 2 mTorr and a current

of 1.5 A was obtained at a voltage of 150 V. The axial magnetic field strength was 3000 Gauss. The Bohm diffusion coefficient is given by

$$D_B = \frac{ckT_e}{16eB}. \quad (7)$$

Since the ion temperatures were comparable to T_e in Bohm's experiments ($T_i = 0.5T_e$), the diffusion coefficient for ions was also comparable to that for electrons. The electron density was on the order of 10^{12} cm^{-3} . Even though a formal derivation for the Bohm diffusion coefficient was never published, it was an estimate based on the cross field diffusion expected from self-excited fluctuating fields (turbulence).

The Bohm diffusion coefficient is usually much larger than the classical diffusion coefficient at high magnetic fields. But for fields on the order of 100 Gauss, the reverse is true, and the two diffusion coefficients are equal for a 600-Gauss field for the parameters given below. Specifically, at 100 Gauss $D_B = 1.25 \times 10^5 \text{ cm}^2/\text{s}$ for 2-eV electron temperature. The classical diffusion coefficient $D_{\perp e}$ for electrons may be calculated from $D_{\perp e} = D_{oe}\nu_{me}^2/(\nu_{me}^2 + \omega_{ce}^2)$. At 150 mTorr, $\nu_{me} = 6 \times 10^8 \text{ Hz}$ and at 100 Gauss, $\omega_{ce} = 1.76 \times 10^9 \text{ rad/s}$. Thus $D_{oe} = 5.9 \times 10^6 \text{ cm}^2/\text{s}$ and $D_{\perp e} = 6.1 \times 10^5 \text{ cm}^2/\text{s}$. The classical diffusion coefficient is clearly greater than the Bohm diffusion coefficient for electrons at 100 Gauss. An estimate of the ambipolar diffusion coefficient may therefore be made by using the classical diffusion coefficients for electrons and ions. For ions, $\nu_{mi} = 2 \times 10^6 \text{ Hz}$ and $\omega_{ci} = 3.4 \times 10^4 \text{ rad/s}$. Since $\nu_{mi} \gg \omega_{ci}$, $D_{\perp i} \approx D_{oi} = kT_i/(m_i\nu_{mi}) = kT_i\mu_{oi}/e = 8.58 \times 10^2 \text{ cm}^2/\text{s}$. Also, $\mu_{\perp i} \approx \mu_{oi} = 1.78 \times 10^4 \text{ cm}^2\text{V}^{-1}\text{s}^{-1}$. For electrons, $D_{\perp e} = 6.1 \times 10^5 \text{ cm}^2/\text{s}$ and $\mu_{\perp e} = 3.1 \times 10^5 \text{ cm}^2\text{V}^{-1}\text{s}^{-1}$ using Eq. (5). Substituting the various terms in Eq. (4), $D_a = 3.37 \times 10^4 \text{ cm}^2/\text{s}$.

Based upon the knowledge of D_a , the magnitudes of the three terms in Eq. (2) can be compared. If the central density decays from $2 \times 10^{12} \text{ cm}^{-3}$ to zero in 0.5 cm, then the magnitude of the diffusion term $D_a \partial^2 n / \partial x^2$ is roughly $1 \times 10^{17} \text{ cm}^{-3} \text{s}^{-1}$. The magnitude of the ionization term $\nu_i n$ is $1.2 \times 10^{17} \text{ cm}^{-3} \text{s}^{-1}$ which also applies for the magnitude of the recombination term βn^2 . Thus all three terms can be important in the positive column of the agile mirror plasma. However, D_a will be smaller if T_e is less than 2 eV in which case the importance of the diffusion term may not be very significant. The relevance of the diffusion term will be discussed in Section A6.

It is evident from the numbers quoted above that the term $\mu_{\perp e} D_{\perp i}$ in Eq. (4) can be neglected. Also, $\mu_{\perp i} \approx \mu_{oi}$ for ions. Equation (4) then assumes the simplified form:

$$D_a \approx \frac{kT_e}{m_e \nu_{me} \left(1 + \frac{\omega_{pe}^2}{\nu_{me}^2} \right) + m_i \nu_{mi}}. \quad (4a)$$

This equation shows more clearly the dependence of D_a on electron temperature and magnetic field. An interesting observation made in Ref. 4 is that D_a in the absence of magnetic fields is only slightly larger than that at 100 Gauss. Specifically, $D_a = 3.5 \times 10^4 \text{ cm}^2/\text{s}$ in the absence of magnetic fields, and $D_a = 3.37 \times 10^4 \text{ cm}^2/\text{s}$ at 100 Gauss. However, large differences are observed in the experiment. At 100 Gauss, the glow discharge appears to be essentially planar, while at zero field, the discharge takes on a diffuse form and almost spans the entire chamber diameter near the anode. It would therefore appear that diffusion is not the sole cause of spreading. One explanation for the large differences observed is the possibility that electrons with energies approaching the cathode fall voltage (typically 1.4 kV — see Section B3) propagate the complete length of the positive column

because the collision probability is substantially smaller for higher energy electrons. In the absence of magnetic fields, these "primary" electrons are largely unaffected by the small electric fields within the positive column, and they proceed along directions they were launched initially from the cathode. Electrons emitted from the inside flat face of the hollow cathode proceed essentially parallel to the cathode-anode axis, but they may have some perpendicular velocity after entering the positive column. Electrons emitted from the sides and tips of the hollow cathode may come off at substantial angles. The "secondary" electrons with intermediate energies (tens of eV) generated in the negative glow region, also enter the positive column with substantial angles. This situation is not likely to change even if nonemitting cathode plates are added to impose a uniform vacuum electrostatic field between the cathode and anode planes, because the electric field distribution in the discharge is determined self-consistently by the discharge itself and most of the voltage drop occurs very close to the hollow cathode. When a 100-Gauss magnetic field is added, the high energy electrons are forced to gyrate around magnetic field lines. The gyroradius of a 1.4 keV electron is 0.8 cm if, say, half its energy is assumed to be in the perpendicular motion. This is consistent with the observed 1-cm width of the discharge column at 100 Gauss.

Equation (1) is therefore not applicable to this beam produced plasma. It is still valid for a thermal plasma, and the method of solution is outlined in Ref. 4. It is possible that a hollow cathode with different proportions operating at a higher pressure may yield a thermal plasma with electron densities on the order of 10^{12} cm^{-3} . The ambipolar diffusion coefficient D_a would then determine the width of the discharge column. A higher magnetic

field should lower the diffusion coefficient, and hence the discharge width. Using Eq. (4a), it may be verified that a 450-Gauss field is needed to reduce D_a to half the zero field value.

4. Ion Gyroradius

The axial magnetic field in Figs. 7(b), 8(b) and 9(a) is roughly 100 Gauss. If the ions are assumed to be at room temperature, namely 300°K, then the ion gyroradius is 0.9 cm and the diameter of the gyro orbit is 1.8 cm. However, $\nu_{mi} = 2 \times 10^6$ Hz and $\omega_{ci} = 3.4 \times 10^4$ rad/s. Since $\nu_{mi} \gg \omega_{ci}$, collisions swamp the gyro motion and the magnetic field has little influence on the ion motion.

5. Filamentation

Filamentation is observed at elevated pressures in gas laser plasmas where an axial magnetic field is usually not employed. If filamentation develops within the positive column of the agile mirror discharge, the reflective qualities of the mirror would be degraded appreciably. The axial magnetic field employed in agile mirror discharges, facilitates the development of a uniform planar discharge from the hollow cathode (see Section B1). It is therefore quite possible that filamentation can occur only if the initiating mechanisms for it are found within the positive column. Gas heating initiates filamentation in gas laser plasmas. If the gas is heated appreciably, say, to twice the original temperature, the discharge column may contract into a filament (or filaments in the case of planar discharges). When the local temperature of the gas rises, the gas density falls since the heating occurs at constant pressure. This raises E/N , and as a result the electron temperature and electron density rise. The increased plasma conductivity causes the current density to rise

which in turn raises the local temperature, and the cycle repeats.

The threshold current and electron densities above which filamentation could occur in laser plasmas are³ $j_o = 0.17/p$ A/cm² and $n_{eo} = 6 \times 10^{11}/p$ cm⁻³. For $p = 0.15$ Torr, the threshold densities are 1.1 A/cm² and 4×10^{12} cm⁻³. This means that for some of the data in Figs. 7 thru 9, the discharge may be close to the threshold for filamentation, but it is not known if these thresholds are strictly valid for magnetized plasmas.

6. Interpretation of Data

The reflected microwave signal does not have a flat time profile in Figs. 7 thru 9, and in some cases it does not last as long as the voltage pulse. A distinction needs to be made between problems caused by the hollow cathode, and problems in the positive column that are to a great extent unrelated to the manner in which a discharge is initiated at the cathode. For example, in Fig. 7(c) the microwave signal turns off at $\sim 150 \mu\text{s}$ because the discharge current has dropped appreciably. The electron density is below the threshold for reflection in the low current state. The turn-off phenomenon is directly traceable to problems in the hollow cathode, because clearly if there is no current there is no mirror to reflect microwaves off. In contrast, Fig. 9(b) shows a case where the discharge current is reasonably flat, yet the microwave signal has large amplitude, low frequency oscillations. This is most probably caused by imperfections in the positive column. The hollow cathode problem will not be addressed in this section. It will be treated later, after the discussion on the cathode layer.

The reflected microwave signals (see Figs. 7 thru 9) increase in amplitude and flatten out as the magnetic field is raised to 163 Gauss. (The maximum field that could be

obtained with the coil power supply was 163 Gauss). Also, the magnetic field required to obtain reasonably large reflected signals increases as the discharge current or pressure increases. One explanation for this behavior is that at low magnetic fields, the high energy electrons are not well confined. Additionally, as the discharge current rises the electron temperature also rises, which increases the diffusion coefficient of the thermal plasma (see Section A3). The magnetic field required to confine the column rises as a result. Thus a higher magnetic field improves the confinement of both the high energy electrons and the thermal plasma. It is quite possible that at low magnetic fields, the spreading of the discharge is severe enough that the critical (reflecting) surface is no longer flat. It may fan out like a wedge or it may be rough (on the scale of the microwave wavelength). The reflected microwave signals which depend critically on the shape of the reflecting surface therefore show appreciable magnetic field dependences.

An interesting feature about the data is that in some cases there is no thru-transmission when the reflected signal is also small. The absorption coefficient η in a plasma is given by $\eta = \omega_p^2 \nu_{me} / [c(\omega^2 + \nu_{me}^2)]$, where ω_p is the plasma frequency and $\omega_p^2 = 4\pi n e^2 / m_e$. At 183 mTorr, $\nu_{me} = 7.3 \times 10^8$ Hz. For 10-GHz microwaves and 10^{12} -cm $^{-3}$ density, $\eta = 0.022$ cm $^{-1}$. It would therefore take a 46-cm thick plasma slab to attenuate the incident microwave radiation to 37 % of the incident power level. Thus microwave absorption is negligible when the positive column spreads out due to diffusion. It must be that the critical surface is reflecting microwaves specularly in different directions, or that the reflection from the mirror is like the diffuse reflection from a rough surface. This could explain why both the reflected and transmitted signals are small.

B. CATHODE LAYER

In the positive column most of the current is carried by electrons. But very near the cathode most of the current is carried by ions, a majority of which are created close to the cathode by electron impact ionization of gas atoms. In an arc, the intense bombardment of the cathode by ions raises the surface temperature to very high levels and thermionic emission is the primary means of electron production. In a normal glow, secondary emission of electrons occurs when ions impact the cathode surface. This mechanism is extremely inefficient when compared with thermionic emission. The secondary emission coefficient γ represents the number of electrons emitted from the cathode surface by one incident ion. Its value depends on the cathode material and the type of gas employed. It is almost independent of the incident ion energy up to energies close to 1 keV. It ranges in value from 0.01 to 0.2. The available data on γ are incomplete and often contradictory, partly because contaminated surfaces yield very different values. In a hollow cathode there are some indications that ultra-violet light induced photoelectric emission may also be important.⁸

E/p in the positive column was found to be $2.5 \text{ V cm}^{-1}\text{Torr}^{-1}$ (see Section A2). Therefore, the voltage drop across the 25-cm long column at 150 mTorr is 9.4 V, which is negligible compared to the discharge voltage of 1.4 kV. The cathode fall is thus almost 1.4 kV. Assuming the 8-Amp discharge current is uniformly distributed across the hollow cathode surface, the current density at the cathode surface is nearly 0.13 A/cm^2 .

1. Hollow Cathode

A hollow cathode may take the form of a hollow cylinder, a spherical segment, a

deep groove in a cathode plate, or simply a pair of plane-parallel plates. In all cases, the pressure must be such that the cathode layer thickness is comparable to the intercathode separation. This causes the negative glows of the cathodes to interact. In the absence of an external magnetic field, the faster electrons from the dark space of one cathode penetrate the glow of the opposite cathode, where they are decelerated, reverse their paths, and repenetrate their own glow. As the two cathode surfaces approach each other the number of fast electrons that reflex between the two glows increases substantially. Thus, a large proportion of the energy of the faster electron swarms in the cathode fall is efficiently used in creating new positive ions⁹, with the result that the current rises for the same cathode fall.

In hollow cathode arcs, the primary reason for using a hollow cylinder as a cathode is to increase the surface area for handling the much higher current densities with minimal erosion. The length to diameter ratio must be at least 6:1 for efficient operation¹⁰ of the hollow cathode arc. Most of the earlier hollow cathodes extended the normal regime of a glow discharge.¹¹⁻¹³ Current densities were on the order of 10 mA/cm^2 . Figure 13 shows the V-I characteristics of a hollow cathode,¹³⁻¹⁴ and a plane cathode operating in the abnormal glow regime. It shows that for the same cathode fall V_c , the current density may be hundred times larger than for a plane cathode.

A more recent hollow cathode discharge attained surface current densities in excess of 0.5 A/cm^2 in the "glow" mode.¹⁵ The cathode was a 0.75-mm-diam. cavity inside a refractory metal electrode. The cavity had a 0.185-mm-diam. aperture which faced the anode. The cathode operated at 10 mA in neon at a pressure of 100 Torr. The current

density at the cavity surface was $\sim 0.5 \text{ A/cm}^2$ and it was as high as 30 A/cm^2 at the plane defined by the aperture. The cathode fall V_c was 115 V.

The presence of an external magnetic field complicates the operation of the hollow cathode. The agile mirror cathode is presently a rectangular channel in a brass electrode. High energy electrons emitted from the inside flat face of the cathode do not play an important role in the hollow cathode effect caused by the interacting negative glows. They do, however, influence the nature and shape of the positive column. Electrons emitted from the sides of the cathode typically have energies on the order of 1.4 keV, corresponding to the cathode fall voltage. A 100-Gauss magnetic field parallel to the anode-cathode axis, limits the gyroradius of the 1.4-keV electrons to 1.2 cm. Thus, instead of reflexing between the two negative glows, these electrons perform a "cycloidal" motion within the cathode hollow. Electrons emitted by one of the sides drift within the hollow from, say, left to right, while those from the other side drift from right to left. This motion substantially increases the probability of ionization of the background gas. It also facilitates the generation of a uniform planar discharge because the motion smoothes out nonuniformities in the hollow cathode emission. The secondary and subsequent generations of electrons created within the two negative glows also interact if the hollow cathode dimensions are appropriately chosen. Since the magnetic field strength determines the scale length of the "cycloidal orbits", it is conceivable that for a given gas pressure, there is an optimum magnetic field strength and an optimum intercathode separation for efficient hollow cathode operation.

2. Sputtering

Sputtering refers to the ejection of neutral cathode material atoms due to the bom-

bardment of the cathode surface by ions from the glow discharge. Many of the seemingly contradictory results obtained with hollow cathodes are traceable to the effects of sputtering.¹⁵ At high current densities, the high sputtering rate and the nonuniform flow of sputtered material within the hollow results in the alteration of the internal configuration of the cathode by the discharge. In addition, large numbers of gas atoms are trapped in the sputtered material. In a typical case 1.6×10^{15} atoms/cm² were deposited, which corresponds to 1000 monolayers of adsorbed gas atoms.¹⁵ Sputtering may be important in agile mirror discharges because the release of adsorbed gas atoms and sputtered cathode material could result in a high gas density early in time.

The mass m sputtered in unit time is empirically given by the relation⁹ $m = a(V_c - K_o)$, where a and K_o are constants and V_c is the cathode fall. K_o represents the threshold above which substantial sputtering occurs, and the value of K_o for most materials ranges from 400 to 600 V, which is well above the *normal* cathode fall of most metals. But when the current density is increased with the cathode fully covered by the glow, the abnormal cathode drop at high V_c may cause sputtering to occur.

3. Cathode Fall

Figure 13 shows the dependence of the cathode fall V_c on the discharge current for the parallel-plate hollow cathode in Ref. 13. At low currents, the discharge operates in the abnormal glow regime, where V_c increases with j . At roughly 1 mA/cm², the discharge transitions into the hollow cathode mode. A recent paper¹⁶ reported such transitions in a pulsed hollow cathode discharge. However, the transitions were suppressed when the axial magnetic field exceeded 1500 Gauss. A somewhat unrelated aspect of glow discharges

concerns the difference between the dynamic V-I characteristics at low and high frequencies. A glow discharge operating in the *normal* regime at low frequencies, adjusts the emitting surface area keeping the current density constant, when the discharge current rises. This explains why the V-I characteristic for a normal glow is a horizontal line. At frequencies above 2 kHz, the glow area cannot change as fast as the current does, with the result that the area A remains essentially fixed, and the normal glow voltage increases with current.¹⁵

The V-I characteristics for the agile mirror plasma appear in Fig. 4. They were obtained from a sequence of shots with different parameters, and are similar in shape to the hollow cathode characteristic appearing in Fig. 13. The cathode fall is roughly 1.4 kV for a discharge current of 8 A. This appears to be a large voltage drop, especially in view of the fact that surface current densities in excess of 0.5 A/cm^2 were obtained with V_c as low as 115 V in Ref. 15. Sputtering is certainly occurring in the agile mirror cathode. This was evident upon a visual observation of the cathode hollow after months of operation. Damage due to sputtering was observed on the inside flat face and the two sides of the cathode hollow. No damage was observed near the inside corners and the two ends of the cathode cavity, and the transition from the damaged to the undamaged areas was quite smooth. The cathode hollow is 1.2 cm deep and 1.6 cm wide. Most hollow cathodes employ cavities with depth much greater than the width. It is quite possible that the present cathode is not efficiently performing in the hollow cathode mode. It may be operating in a transitional regime between the abnormal glow and hollow cathode modes. A worthwhile experiment to perform would be to increase the depth of the cathode hollow by at least a factor of two and determine the characteristics of the mirror. The fact that sputtering occurs over

the recessed flat face of the hollow cathode confirms the suspicion that the cathode cavity is not deep enough. A deeper cavity should facilitate increased interaction between the two negative glows. It will also provide increased cathode surface area resulting in higher currents and a much lower cathode fall. It may also delay the current turn-off phenomenon observed under a wide range of experimental parameters (see Section B7 below).

Theories describing the cathode fall in a normal glow¹⁷ and in a hollow cathode⁸ are not applicable when the current density at the cathode surface exceeds 0.1 A/cm^2 . Both theories predict ridiculously low values of current density for a cathode fall of 1.4 kV. The plasma acts like a grid placed less than a millimeter from the cathode. The entire cathode fall occurs across a layer less than a millimeter thick. The electric field is on the order of 10 kV/cm in this layer. Tabulated values for the drift velocity, ionization coefficient, etc. are not valid in the cathode layer because the electric fields and gradients are so high. Large uncertainties are also associated with the various other physical processes occurring in the layer. The current density can no longer be calculated self-consistently. However, if the cathode fall and current density are known, the cathode fall thickness can be calculated. Following the treatment in Ref. 15, two relevant theories are outlined below, which enable the computation of the cathode fall thickness.

A cathode fall of 1.4 kV implies that electrons emitted from the cathode exit the collisionless cathode layer with energies corresponding to the full cathode fall voltage. Most of the electrons coming off the recessed flat face of the hollow cathode enter the positive column and may even reach the anode. Electron energy distributions measured in abnormal glow discharges at pressures in the range 3 – 25 Torr, are found to be distinctly

non-Maxwellian.¹⁸ In particular, the distribution in the negative glow close to the cathode dark space shows a prominent tail of high energy electrons, and a beam component at the cathode fall voltage. However, the tail and beam components are totally absent in the positive column. Measurements of energy spectra of electrons arriving at the anode in a 3-kV, 60-mA, argon discharge at 10 mTorr, show that roughly 40 % of the 60-mA current is carried by high energy electrons,¹⁹ namely those with energies exceeding 300 eV. The spectrum also shows that the electron distribution is skewed towards the high energy end, and the largest percentage of fast electrons reaching the anode have energies approaching 3 keV. The pressure of the background gas in typical agile mirror discharges is 150 mTorr. Based upon the measurements in Refs. 18 and 19, the percentage of the discharge current carried by high energy electrons in agile mirror discharges is probably somewhere between zero and 40 %. The fast electrons could also profoundly influence the density and temperature of the positive column. The details of the energy exchange mechanisms between the fast electrons and the background plasma are not well understood.²⁰ Besides electron impact ionization and Coulomb interaction between the slow and fast electrons, energy exchange can also take place via plasma waves²¹ because beams with velocities far above the mean thermal speed introduce a tendency towards instability so that small oscillations grow until limited by nonlinear effects.

4. Free Fall Theory

The free fall theory assumes that positive ions move from the negative glow to the cathode without collisions of any kind. Under these conditions, the field in the cathode region can be calculated from a solution of the two equations $\nabla \cdot E = d^2V/dz^2 = 4\pi\rho$ and

$eV = M_i v_i^2 / 2$, where M_i is the ion mass. If γ is the ratio of the electron current emitted from the cathode to the positive ion current striking it, then the cathode fall V_c is related to the current density and the cathode fall thickness z via the relation²²

$$z^2 = \frac{(1 + \gamma)}{9\pi j} \sqrt{\frac{2e}{M_i}} V_c^{3/2}. \quad (8)$$

The electric field dependence in this layer is then $E \sim z^{1/3}$, where the boundary conditions are $E = V = 0$ at $z = 0$ which is the cathode edge of the negative glow.

If the $(1 + \gamma)$ term is dropped, Eq. (8) is identical to the collisionless Child-Langmuir relation for a space charge limited ion diode. Here, the plasma acts as the emitter of space charge limited ion current, and the cathode plays the role of the collector. Using a typical value of 0.1 for γ , the cathode fall thickness z is 0.67 mm for $V_c = 1.4$ kV and $j = 0.13$ A/cm². At 150 mTorr, the electron mean free path is 2 mm for electron energies less than 10 eV, and the ion mean free path is 0.1 mm. High energy electrons have much larger mean free paths. Even though there are no electron collisions within the cathode fall layer, there are several ion collisions. So the basic assumption that the ions move from the glow to the cathode without collisions, is not strictly valid.

5. Mobility Theory

E/p in the cathode fall layer is on the order of 10^5 V cm⁻¹Torr⁻¹. There is no experimental data available for ion mobility at such high values of E/p . The average velocity of positive ions in a gas is determined by collisions with gas molecules, and charge exchange collisions can be important. At low values of E/p the ion velocity varies as

E/p , but at high values (around 1000 V cm⁻¹Torr⁻¹) the velocity varies as $\sqrt{E/p}$, i.e. $v_i = k'_i \sqrt{E/p}$, where k'_i is a constant for each gas and is now called the mobility. By using this dependence, the cathode fall thickness is given by²²

$$z^{5/2} = \frac{5}{3j} \left[\frac{1.147(1 + \gamma)}{6\pi} \sqrt{\frac{e\lambda_i}{M_i}} \right] V_c^{3/2}, \quad (9)$$

where λ_i is the ionic mean free path and M_i is the ion mass. The electric field distribution is $E \sim z^{2/3}$, where $z = 0$ is the cathode edge of the glow.

The ion mean free path is 0.1 mm at 150 mTorr. Using $\gamma = 0.1$, $V_c = 1.4$ kV and $j = 0.13$ A/cm² the cathode fall thickness z is 0.62 mm, which is close to the value of 0.67 mm calculated in the previous subsection. The agreement is probably coincidental. The electron mean free path is 2 mm for electrons with energies less than 10 eV, which means there are no electron collisions within the cathode fall layer.

6. Self Sustainment Condition

All the ions reaching the cathode are created by electron impact ionization of gas atoms. If there are no electron collisions within the cathode fall layer, all the ions must have been created outside the layer. Although most of the voltage drop occurs across the cathode fall layer, there is substantial electric field outside the layer. α/p is an increasing function of E/p , α being the Townsend ionization coefficient. Since the electric field decays away from the cathode fall layer, α/p also decreases with distance within the negative glow. The self sustainment condition for a glow discharge is³

$$\int_0^L \alpha(E) dz = \ln \left(1 + \frac{1}{\gamma} \right). \quad (10)$$

This equation expresses the fact that a specific number of generations have to be produced in the electron avalanche. This number is determined only by γ and is independent of whether the field is homogeneous or not. An electron starting from the cathode needs to generate enough ions which upon reaching the cathode cause the emission of at least one electron to keep the discharge alive.

For the sake of simplicity, α may be considered a constant over the integration length. Then $\alpha L = \ln(1 + 1/\gamma)$. Taking $\alpha/p = 10 \text{ cm}^{-1}\text{Torr}^{-1}$ for air at $E/p > 1000 \text{ V cm}^{-1}\text{Torr}^{-1}$, and taking $\gamma = 0.1$, $L = 1.6 \text{ cm}$. This gives an order of magnitude estimate of the width of the negative glow. This also determines the intercathode separation desired for achieving substantial interaction between the two negative glows in a hollow cathode. Since the electron mean free path is 0.2 cm, eight generations are produced in the electron avalanche in the 1.6-cm wide negative glow. The length L cannot be arbitrarily large. Since $\alpha(E)$ decreases with distance, the value of the integral in Eq. (10) ceases to increase at large distances. Another problem concerns the ionization coefficient α that is needed in Eq. (10). The Townsend coefficient is taken from experimental data on ionization in homogeneous fields. In the negative glow, the electric field can vary by a factor of 100, the thickness of the glow does not exceed ten mean free paths, and absolute values of E/p can reach $10^4 \text{ V cm}^{-1}\text{Torr}^{-1}$. It is therefore not surprising that the Townsend ionization coefficient ceases to be valid for the negative glow and for the cathode fall regions. Monte Carlo simulations³ of the stochastic processes in the cathode layer solve the kinetic

equation numerically and arrive at a comprehensive picture of the discharge evolution at the cathode. The ionization coefficient is found to be much smaller than the one obtained from the Townsend formula. It is also found that roughly half the electrons are produced beyond the cathode layer in the weak field region.

7. Interpretation of Data

The current turn-off phenomenon deserves some attention. Interestingly enough, a similar phenomenon was observed by Bohm⁷ in the 2-mTorr Argon discharge (see Section A3). Relaxation oscillations were observed at low pressures. The experimental parameters were : Pressure 0.56 mTorr, Magnetic field 3500 Gauss, Voltage 40 V and Current 1.5 A. The period of the oscillations was 850 μ s. The discharge was ON for 280 μ s and it was OFF for the rest of the period. The reason for the oscillations was that the discharge was operating marginally and could be readily extinguished if the ion current reaching the cathode dropped below the level for self sustainment. It was also observed that the threshold for the onset of relaxation oscillations, occurred at a lower pressure when the magnetic field was increased. This was supposedly because a higher magnetic field hampers the diffusion of ions and electrons perpendicular to the field.

Figure 6(a) shows that the turn-off is observed even in the absence of magnetic fields. One possibility is that sputtering causes a release of some of the adsorbed gas atoms resulting in a higher pressure locally (see Section B2). But as time progresses, the pressure decreases and the discharge switches into a low current state. Manheimer and Fernsler⁴ have recently proposed a relaxation model based on a dense plasma in the cathode hollow. Another possibility is that the heating of the gas within the cathode hollow causes the gas

density to decrease with time resulting in the termination of the high current state after a certain time. In all cases, one would expect no turn-off at higher voltages or at higher pressures, which is what is observed.

When the magnetic field is added, it is as if the cathode remembers it had a turn-off problem (see Figs. 7(b) and 7(c)). The discharge operates marginally again. In the presence of a magnetic field the high energy electrons are constrained to perform "cycloidal orbits" within the cathode hollow (see Section B1), so that the hollow cathode effect may not be fully operational and the discharge tends to turn off after about 150 μ s. But when the magnetic field is raised to 163 Gauss, the turn-off feature is much less prominent (see Fig. 7(d)). It is possible that at the higher magnetic field the "cycloids" are tighter and more efficient ionization occurs, while for magnetic fields less than 163 Gauss the scale length of the orbits are so large that the high energy electrons could more readily drift out of the cathode hollow. Another possibility is that at fields above 163 Gauss, the cross-field diffusion of the plasma column is smaller, and larger ion currents reach the cathode thus ensuring a self-sustained discharge. However, at pressures below 183 mTorr the turn-off is observed even at the higher field. Thus, a combination of higher pressures and a higher magnetic field is needed to realize a discharge without interruptions.

It is therefore evident that an external magnetic field parallel to the anode-cathode axis complicates the operation of the hollow cathode. There are three scale lengths involved: the intercathode separation, the width of the negative glows, and the size of the "cycloidal orbits" of the high energy electrons. Efficient hollow cathode operation requires these three scale lengths to satisfy certain relationships among each other, which are also strongly

pressure dependent. Thus it is quite possible that for each combination of pressure and external magnetic field strength, there is an optimum hollow cathode geometry, the main variant being the intercathode separation. It is also possible that a deeper hollow cathode will enable more efficient interaction of the negative glows, thus resulting in interruption-free discharges at lower pressures.

IV. SUMMARY OF RESULTS

Reasonably acceptable reflected signals of the type appearing in Fig. 2 are presently obtained under a narrow range of experimental parameters. The discharge tends to turn-off around $150 \mu\text{s}$, but if the voltage is left on, the discharge restrikes after $\sim 0.5 \text{ ms}$. This suggests that the mirror may be operated at $\sim 1 \text{ kHz}$ rep rate. For faster rep rates, the turn-off problem needs to be overcome. There are some indications that sputtering or local gas heating may be playing a role here. It is also suspected that the dimensions of the hollow cathode cavity are not optimized enough to facilitate adequate interactions between the two negative glows. The presence of an external magnetic field complicates the operation of the hollow cathode. It is conceivable that for each combination of the pressure and the magnetic field strength, there is an optimum hollow cathode geometry. This calls for a systematic study of the effects of varying the pressure, the magnetic field, and the intercathode separation on the discharge parameters. A hollow cathode with an adjustable cavity width is being built to investigate these effects on the scaled up 50 cm \times 50 cm agile mirror experiment. Another planned experiment would employ a much deeper adjustable cathode. A deeper hollow cathode may increase the obtainable current density, lower the cathode fall (thereby reducing sputtering), and enable operation at lower

pressures without discharge current interruptions. Another worthwhile experiment would be to try out an aluminum hollow cathode partly because aluminum has a higher secondary electron emission coefficient compared with brass.

There appear to be some indications that at the lower pressures, the positive column in the agile mirror discharges is beam dominated. To investigate this more fully, a retarding field analyzer is being built to determine the energy spectrum of the electrons reaching the anode. Most of these high energy electrons (beam) are presently being emitted from the recessed flat face of the hollow cathode. (The adjustable cathode will not have this problem because the cathode cavity will be backed by an insulator.) The high energy electrons entering the positive column may have large gyroradii (on the order of a centimeter). A higher magnetic field confines these electrons better. A lower cathode fall reduces the energy of the fast electrons, which also reduces their orbit size. However, designing a hollow cathode to produce a thermal plasma (as opposed to beam dominated plasma) may be a more attractive option, because it makes more efficient use of the magnetic field, in the sense that high field strengths are no longer needed to confine fast electrons. There may also be other cathode designs (besides hollow cathodes) that could function well in the absence of magnetic fields. Finally, plasma reflectors for microwave beams require adequate ion and electron densities to function as a mirror, but there is no current density requirement. It may be possible to achieve desired electron densities at lower currents with noble gases, because their recombination losses are smaller.

ACKNOWLEDGEMENTS

We thank R. Farnsler, W. M. Manheimer and A. E. Robson of the Plasma Physics Division, and Pete Hansen and J. B. Rao of the Radar Division for helpful discussions and comments. We also thank W. Dolinger and A. Darby for assistance in operating the experiment. This work was supported by the Office of Naval Research.

REFERENCES

1. W. M. Manheimer, IEEE Trans. Plasma Sci. **19**, 1228 (1991).
2. A. E. Robson, R. L. Morgan and R. A. Meger, IEEE Trans. Plasma Sci. **20**, 1036 (1992).
3. Y. P. Raizer, *Gas Discharge Physics*, Springer Verlag, Berlin, 1991.
4. W. Manheimer and R. Farnsler, *Theoretical Aspects of the Agile Mirror*, NRL Memo Report NRL/MR/6707-93-7425, 1994.
5. R. Hake and A. Phelps, Phys. Rev. **158**, 70 (1967).
6. N. A. Krall and A. W. Trivelpiece, *Principles of Plasma Physics*, McGraw Hill, New York, 1973.
7. A. Guthrie and R. K. Wakerling, *The Characteristics of Electrical Discharges in Magnetic Fields*, McGraw Hill, New York, 1949.
8. P. F. Little and A. von Engel, Proc. Roy. Soc. London **224**, 209 (1954).
9. L. B. Loeb, *Fundamental Processes of Electrical Discharges in Gases*, John Wiley, New York, 1939.
10. L. M. Lidsky *et al.*, J. App. Phys. **33**, 2490 (1962).
11. A. Guntherschulze, Zeits. f. Phys. **19**, 313 (1923).

12. A. Guntherschulze, Zeits. f. Tech. Phys. **11**, 49 (1930).
13. A. Lompe *et al.*, Ann. d. Phys. **36**, 9 (1939).
14. M. J. Druyvestyn and F. M. Penning, Rev. Mod. Phys. **12**, 87 (1940).
15. A. D. White, J. App. Phys. **30**, 711 (1959).
16. M. T. Ngo *et al.*, IEEE Trans. Plasma Sci. **18**, 669 (1990).
17. V. Engel and Steenbeck, *Electrische Gasentladungen*, Springer, Berlin, 1934.
18. P. Gill and C. E. Webb, J. Phys. D: App. Phys. **10**, 299 (1977).
19. D. J. Ball, J. App. Phys. **43**, 3047 (1972).
20. B. Chapman, *Glow Discharge Processes*, John Wiley, New York, 1980.
21. D. Bohm and E. P. Gross, Phys. Rev. **75**, 1864 (1949).
22. R. Warren, Phys. Rev. **98**, 1658 (1955).

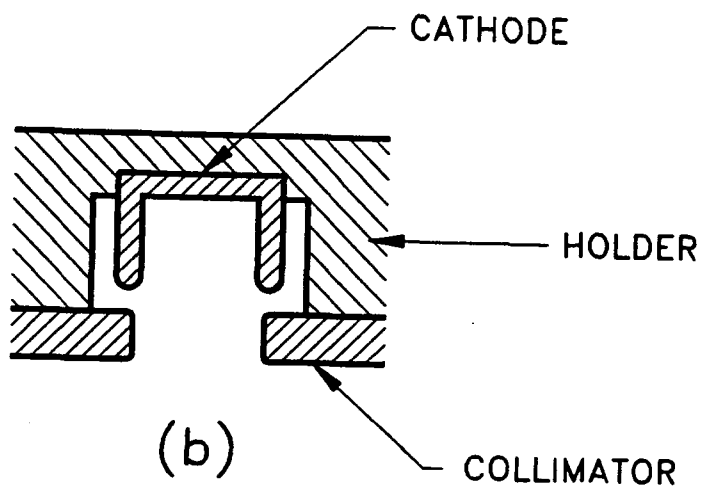
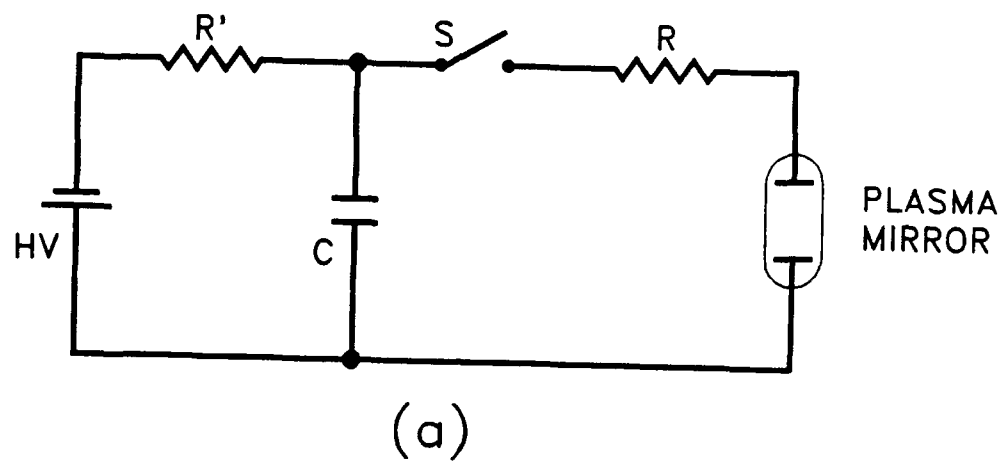


FIG. 1. (a) Simplified circuit diagram of the plasma mirror and its power supply. (b)
Sketch of the hollow cathode assembly.

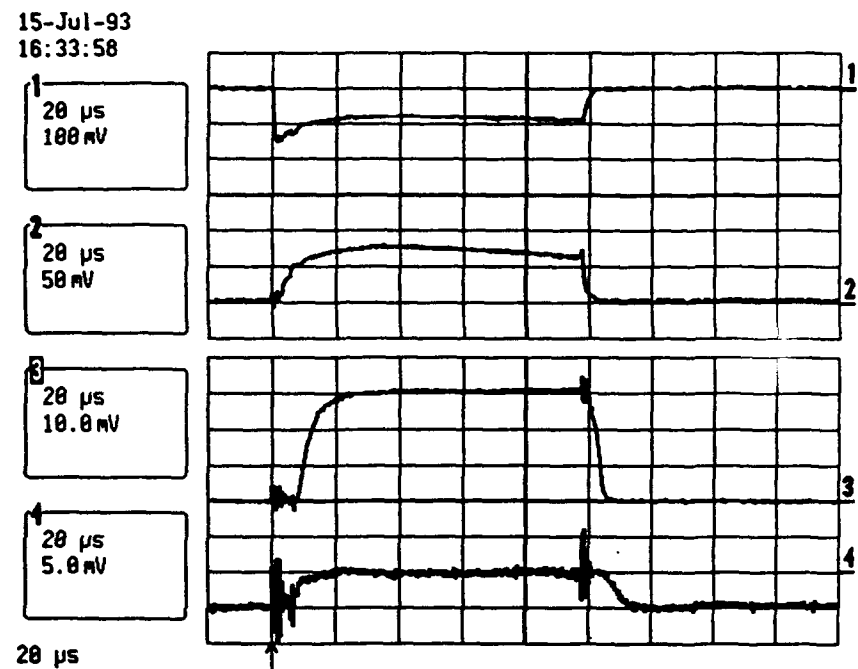


FIG. 2. Agile Mirror data at 150 mTorr and 98 Gauss. The charge voltage is 3 kV, and the series resistance is 180Ω . Ch. 1: Discharge voltage, Ch. 2: Discharge current, Ch. 3: Reflected microwaves, Ch. 4: Thru-transmission.

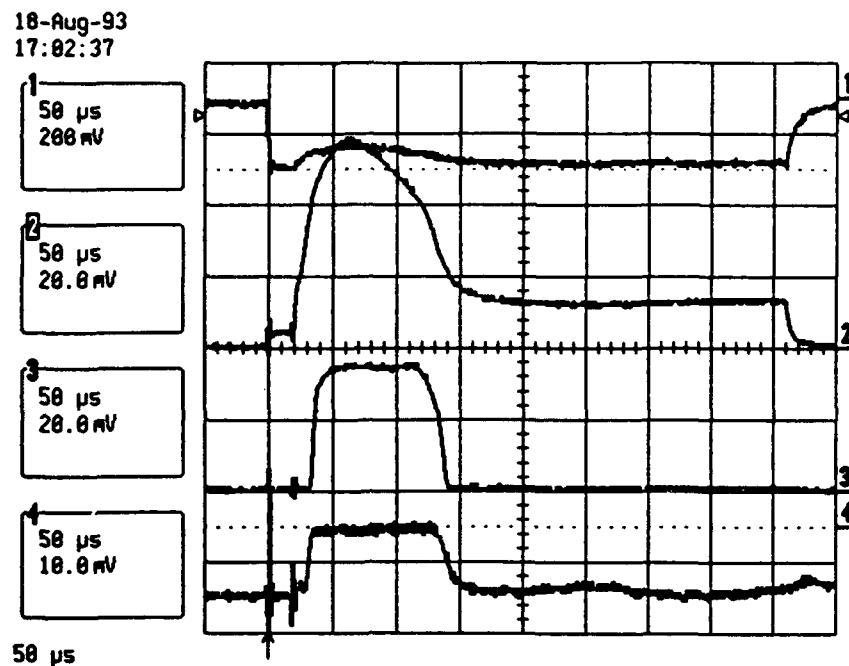
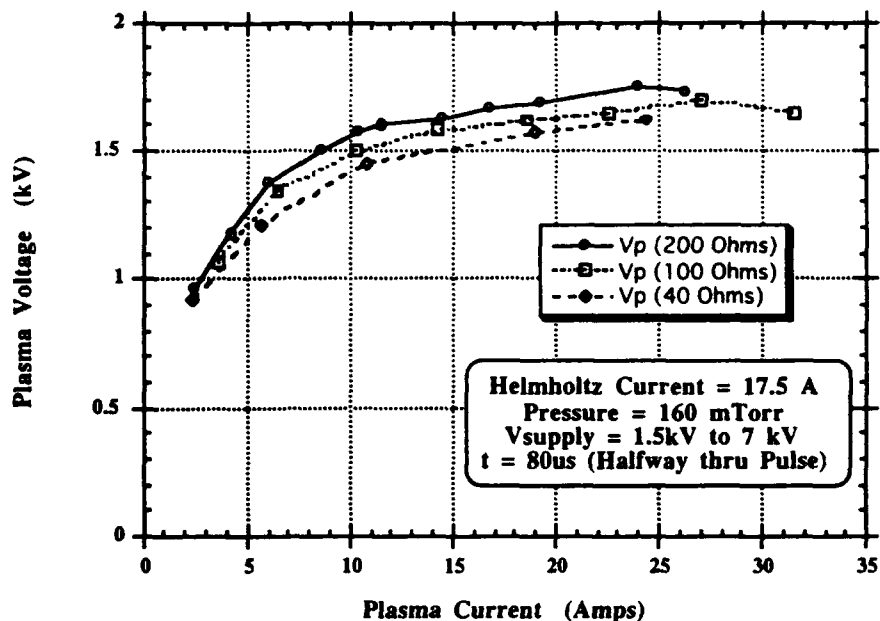


FIG. 3. Data at 158 mTorr and 98 Gauss. The charge voltage is 2.5 kV, and the series resistance is 40Ω . Ch. 1: Discharge voltage - 10 kV/volt, Ch. 2: Discharge current - 100 A/volt, Ch. 3: Reflected microwaves, Ch. 4: Thru-transmission.

(a)



(b)

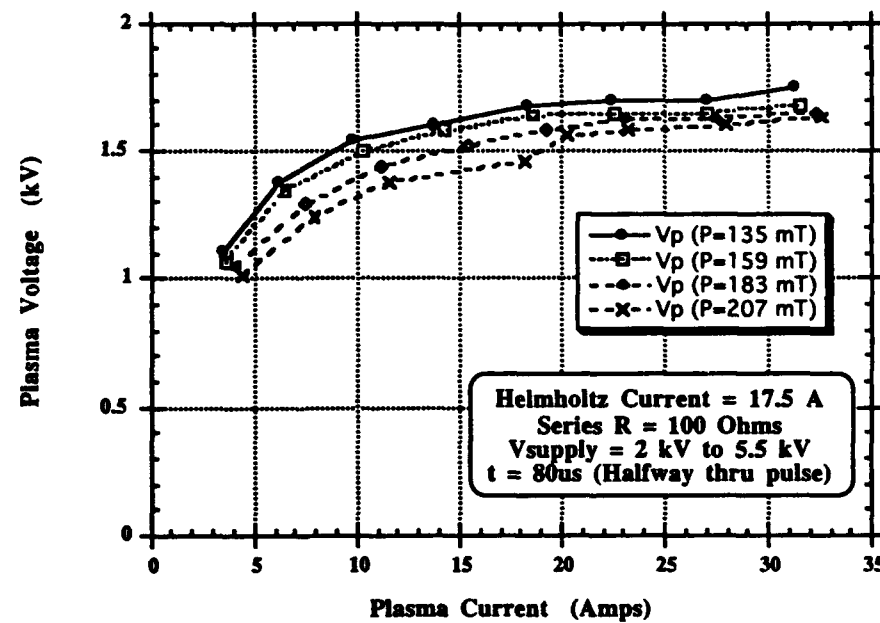
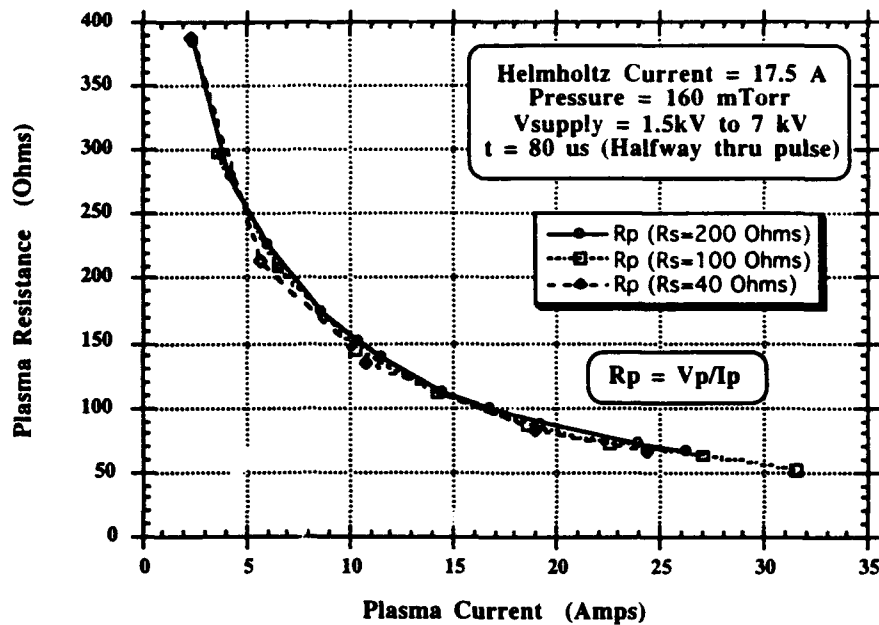


FIG. 4. (a) V-I Characteristics at 160 mTorr for various series resistances. (b) V-I Characteristics for various neutral gas pressures. The series resistance is 100 Ω .

(a)



(b)

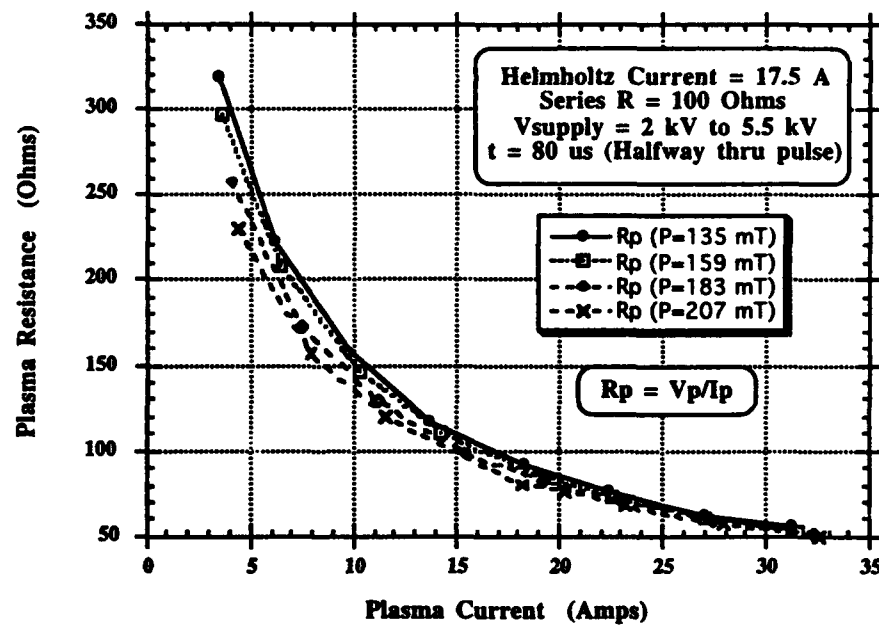


FIG. 5. (a) Plasma resistance at 160 mTorr for various series resistances. (b) Plasma resistance for various neutral gas pressures. The series resistance is 100Ω .

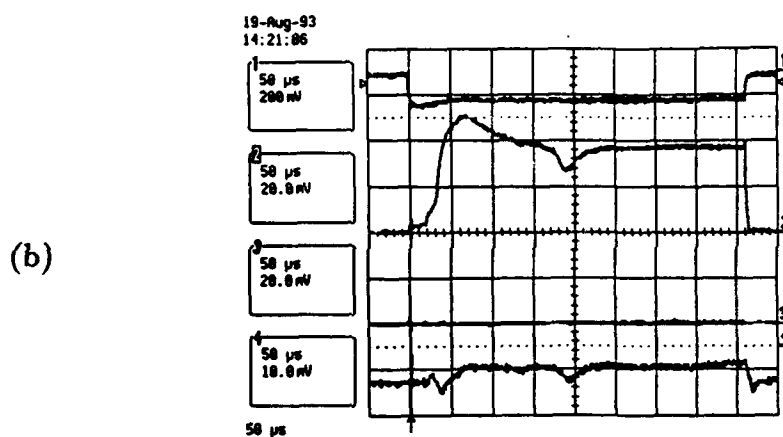
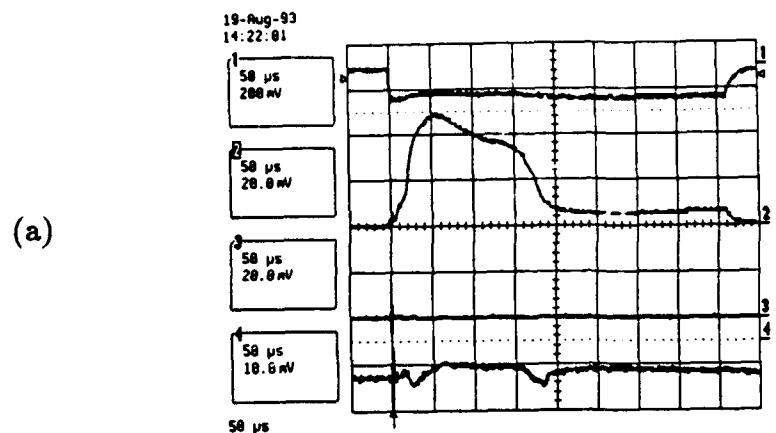
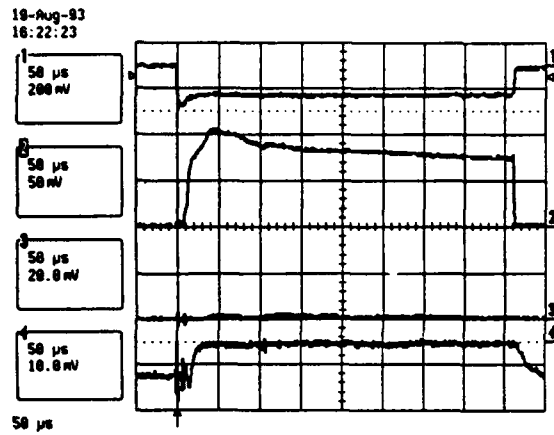
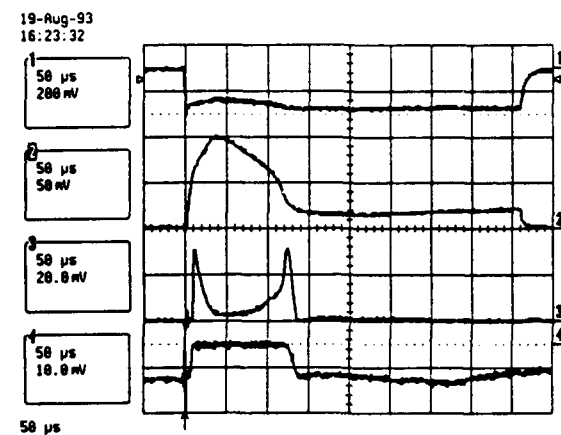


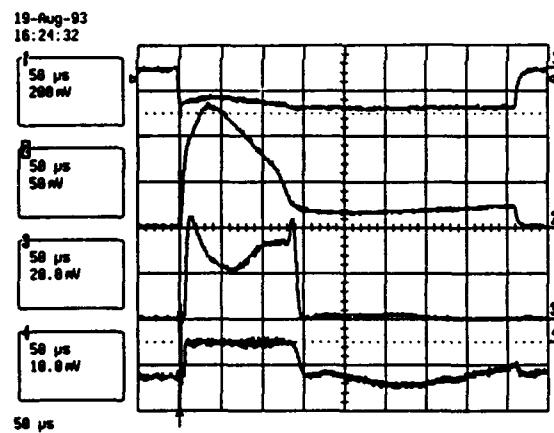
FIG. 6. Two data sets at 158 mTorr and no magnetic field. Charge voltage is 2.0 kV in both cases, and the series resistance is 40Ω . The discharge oscillates between the states (a) and (b).



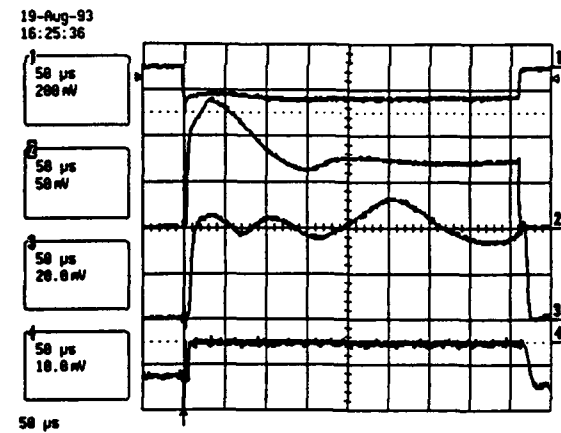
(a)



(b)

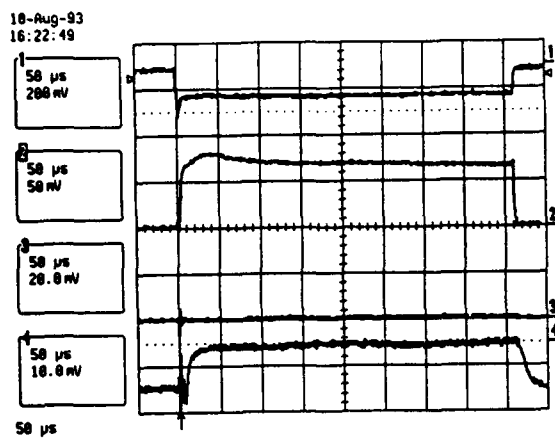


(c)

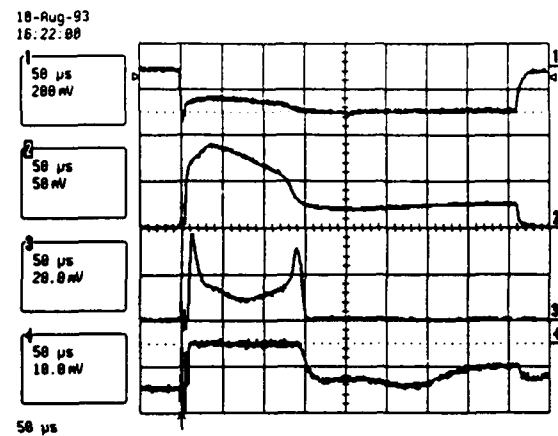


(d)

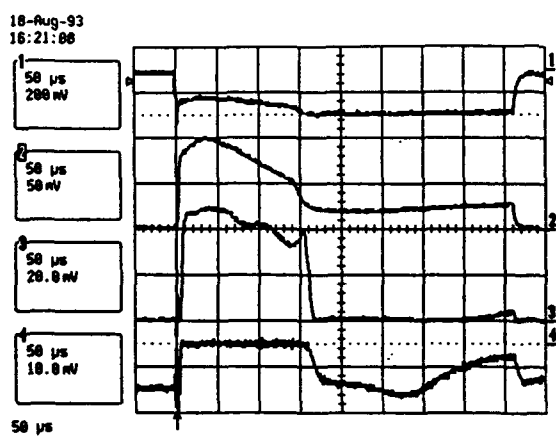
FIG. 7. Data at 183 mTorr and 2.5 kV charge voltage with $40\text{-}\Omega$ series resistance. (a) No magnetic field, (b) 98 Gauss, (c) 130 Gauss, (d) 163 Gauss.



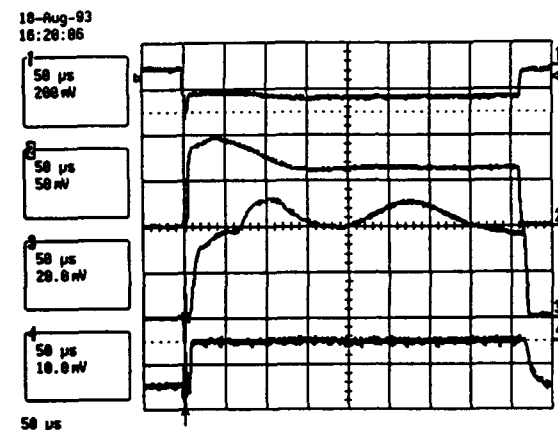
(a)



(b)

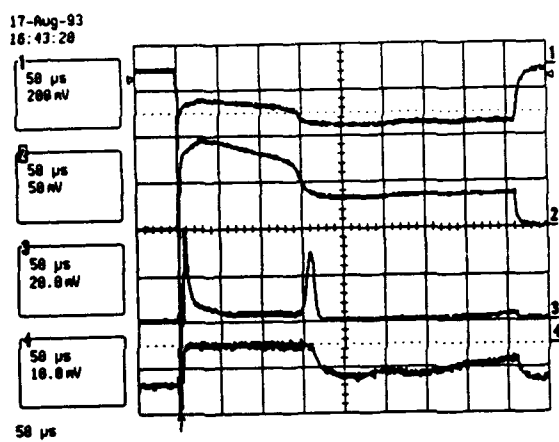


(c)

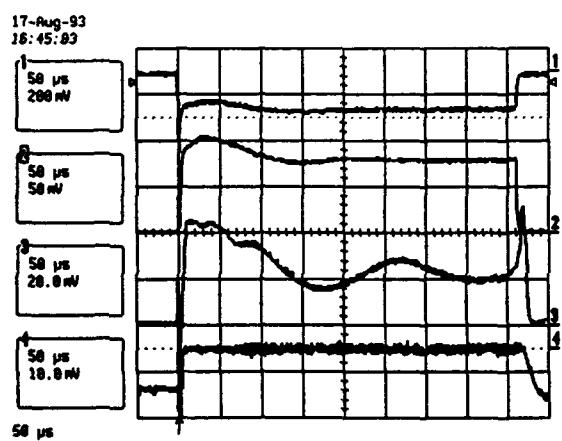


(d)

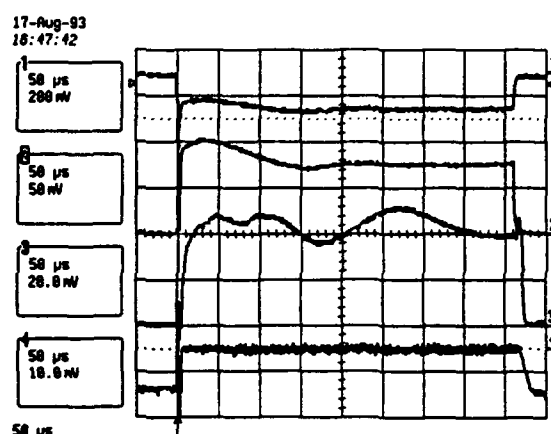
FIG. 8. Data at 183 mTorr and 3.0 kV charge voltage with 100- Ω series resistance. (a) No magnetic field, (b) 98 Gauss, (c) 130 Gauss, (d) 163 Gauss.



(a)

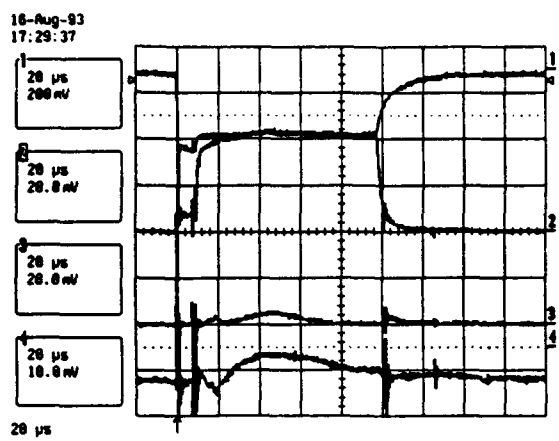


(b)

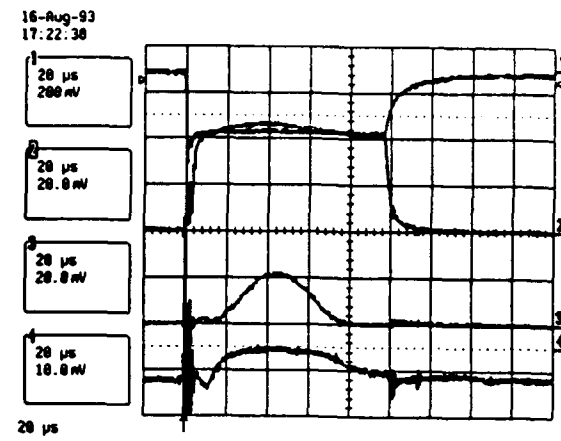


(c)

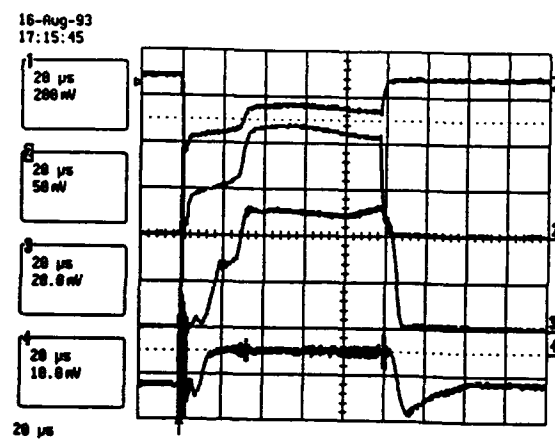
FIG. 9. Data at 183 mTorr and 4.0 kV charge voltage with 200- Ω series resistance. (a) 98 Gauss, (b) 130 Gauss, (c) 163 Gauss.



(a)



(b)



(c)

FIG. 10. Data at 4.1 kV charge voltage and 200- Ω series resistance. Magnetic field strength is 163 Gauss and sweeper frequency is 9.0 GHz. (a) 125 mTorr, (b) 130 mTorr, (c) 138 mTorr.

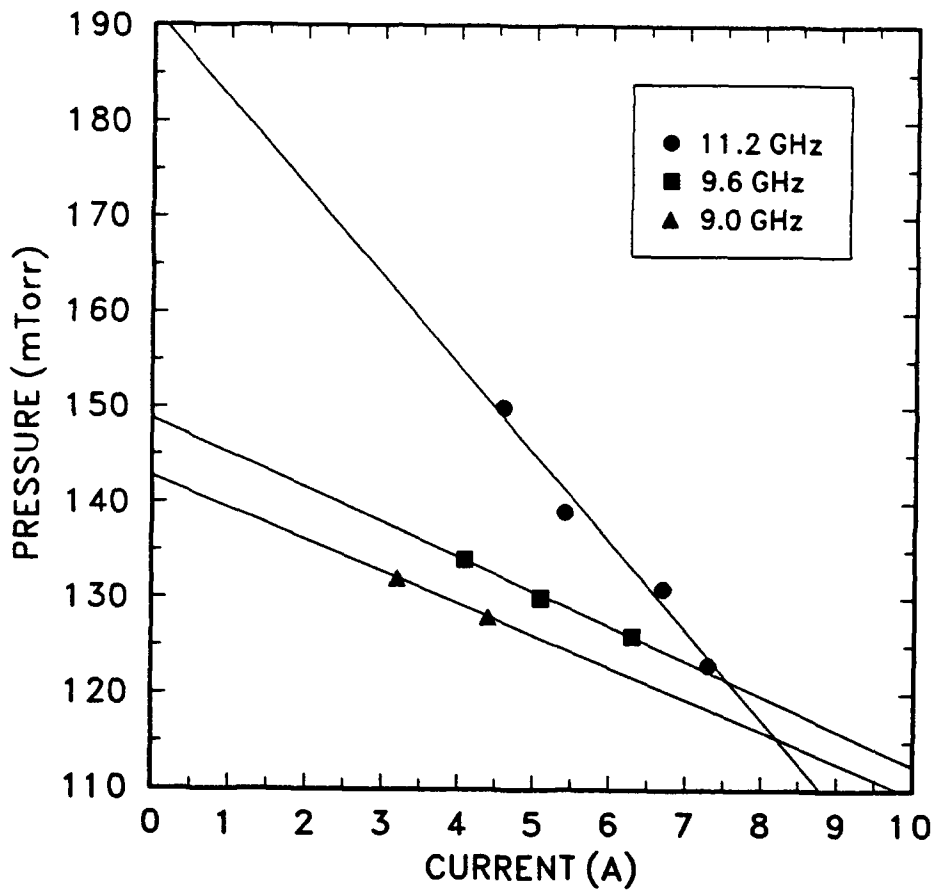


FIG. 11. Locus of points where microwaves begin to be cutoff. The electron densities corresponding to the three microwave frequencies are: 9.0 GHz - 1×10^{12} , 9.6 GHz - 1.14×10^{12} , 11.2 GHz - $1.55 \times 10^{12} \text{ cm}^{-3}$.

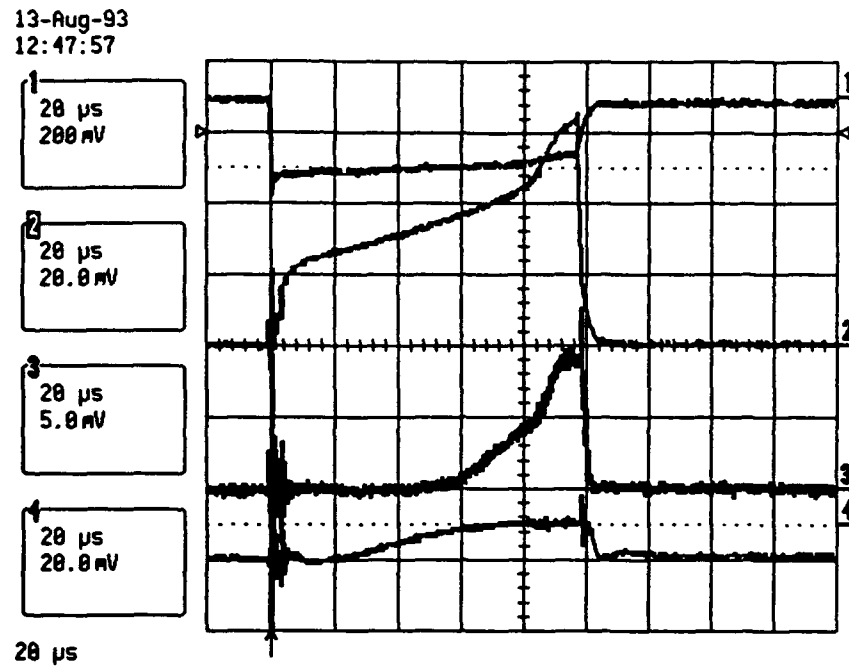


FIG. 12. Data at 3.0 kV charge voltage and $200\text{-}\Omega$ series resistance. Magnetic field strength is 163 Gauss and sweeper frequency is 9.6 GHz. The pressure is 134 mTorr, where the discharge transitions from a low current to a high current state.

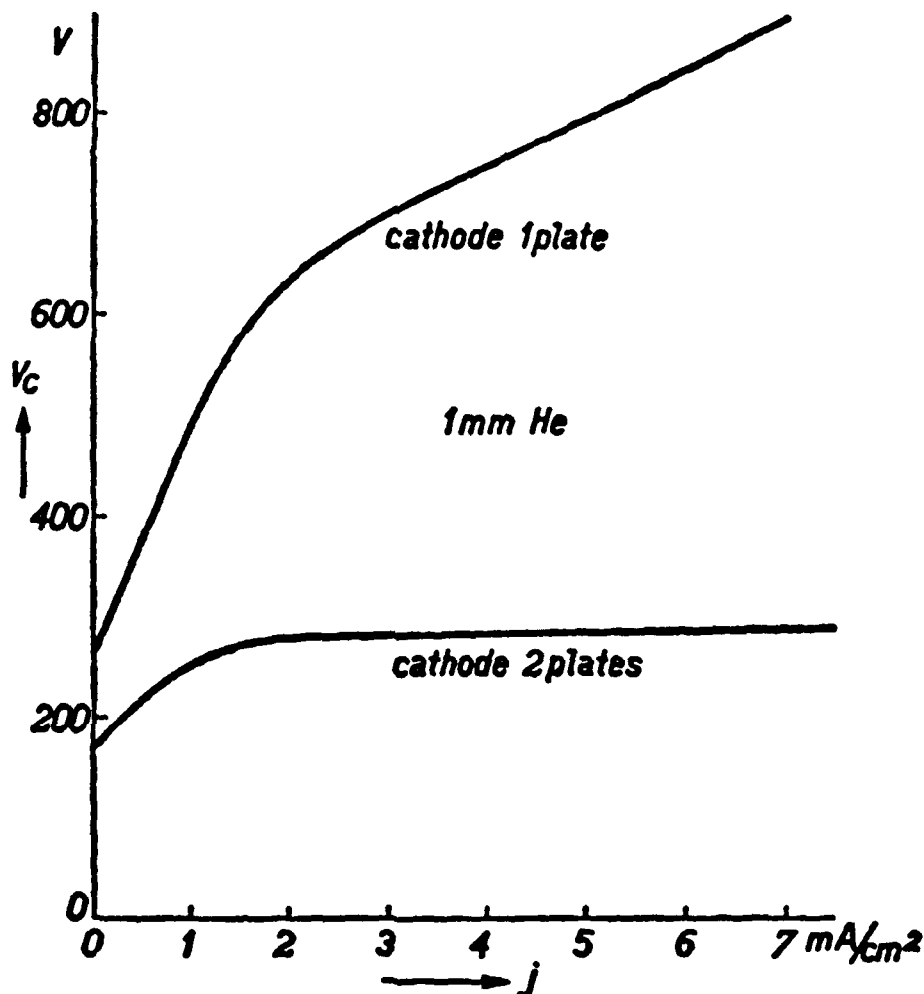


FIG. 13. Cathode fall as a function of current density for single plate abnormal glow and for a two-plate hollow cathode (from Ref. 13).